Optical and Quantum Electronics (2019) 51:307
https://doi.org/10.1007/s11082-019-2014-6

Binocular high dynamic range imaging system based on digital micromirror device

Honghai Sun[1,2] · Yanjie Wang[1,2] · Hang Yang[1] · Pei Wu[1]

Received: 24 June 2019 / Accepted: 22 August 2019 / Published online: 4 September 2019

Abstract
In the applications of scientific imaging and space exploration, the dynamic range of imaging systems is usually required to reach more than 120 dB. In order to observe a highly dynamic scene in real time, we designed an imaging system based on a digital micromirror device (DMD) that is used as a spatial light modulator. First, we designed a binocular highly dynamic light-adjusting system based on a DMD according to the DMD's optical structure. Second, in order to realize the registration between the micromirrors of a DMD and pixels of the two cameras, a pixel-matching algorithm was developed. Finally, we introduce a novel light-adjusting algorithm that can recover the highly dynamic data of the dynamic scene. Experiments showed that the deviation between the DMD and the two cameras is reduced to 0.48 pixels after correction, and that bright and dark targets in a high-dynamic-range scene can both be displayed simultaneously in one image with high quality after light adjustment. The dynamic range of the system is theoretically 209 dB, which meets the requirements of high-dynamic-range observation.

Keywords High dynamic imaging · Image processing · Digital micromirror device

1 Introduction

High-dynamic-range (HDR) imaging, which aims at reproducing images that accurately depict all of the details in wide-range scenes, has attracted increasing attention in recent years. HDR is required in a variety of applications, such as deep-space exploration, solar observation, and the launch process of rockets, missiles, and spacecraft. Obtaining a HDR image presents three challenges: (i) how to extend the dynamic range of the system, (ii) how to realize pixel-level light-adjusting control, and (iii) what kind of algorithm must be applied to capture and reproduce the scene.

✉ Honghai Sun
sunhh426@163.com

[1] Changchun Institute of Optic, Fine Mechanics and Physics, Chinese Academy of Sciences, Changchun 130033, China

[2] Key Laboratory of Airborne Optical Imaging and Measurement, Chinese Academy of Sciences, Changchun 130033, China

HDR imaging technology can be divided into hardware and software methods depending on implementation. The essence of software methods is the multiple-exposures technique, which captures multiple images of the same scene with different exposures and combines the information to build a desired HDR image. This method was first proposed by Mann and Picard (1996) and many conventional algorithms follow it. Huang proposed a histogram-based method to determine exposure time (Huang et al. 2014). Guicquero proposed a novel approach to reconstruct the HDR image from a few compressive measurements (Guicquero et al. 2013). However, such techniques based on multiple exposures have a disadvantage, namely that the captured scene must be completely still.

Hardware methods either expand the dynamic range of sensors or add external optical devices to acquire HDR images. The dynamic range of a sensor is defined as the ratio of the full well capacity (FWC) and the lowest single differentiable from the noise floor (NF). Thus, it can be extended by decreasing NF or increasing FWC (Spivak et al. 2009). However, this method renders sensors that have complex structures, which are expensive, and are not conducive to expanding the resolution. Changing from a linear to a logarithmic response for the photon-electron conversion is another option (Lai et al. 2004; Kavadias et al. 2000). However, in these approaches, spatial resolution will be reduced because some received elements will be considered as a single group. Using a spatial light modulator is one of the most popular current methods of extending the dynamic range of a traditional imaging system. Other researchers have used transmissive liquid crystals (Nayar and Branzoi 2003) or reflective liquid crystals (Mannami et al. 2007) as a device to modulate the scene; however, each of these devices has its own limitations. In transmissive liquid crystals, the driving circuit between the liquid-crystal elements prevents the focus from being on the liquid crystal plane, which means pixel-level adjustment control cannot be achieved. A LCoS is a reflective liquid crystal that has the ability to control attenuation for each imaging pixel, but it cannot be used in binocular imaging systems because of its optical structure. Compared to LCDs and LCoSs, a DMD, a new type of spatial light modulator, has a higher output image signal-to-noise ration (SNR), more stable picture quality, more accurate positioning, and a higher utilization rate of light energy. Some HDR imaging systems based on a DMD (Zhou and Shen 2008; Härter et al. 2011; Reza and Riza 2009) do not take full advantage of a DMD's optical structure.

In this paper, we proposes a binocular HDR imaging system that uses a DMD as a spatial light modulator. A DMD, a programmable device, generates a mask image over the original scene; hence, the scene is regionally modulated. We combine the advantages of software and hardware methods and extend the dynamic range to 209 dB. The binocular system captures two images with different details of the same scene by fully utilizing the optical structure of a DMD. According to the DMD's characteristics, a self-calibration method is put forward that calibrates the system without an external calibration pattern. A light-adjusting algorithm is designed that adjusts the sampling times according to the scene acquired. The rest of the paper is organized as follows. In Sect. 2, the binocular HDR imaging system is introduced. In Sect. 3, we elaborate on the proposed pixel-level self-calibration method, and in Sect. 4 propose the light-adjusting algorithm. Experimental results demonstrating the imaging capability of the system are presented in Sect. 5. We present our conclusions in Sect. 6.

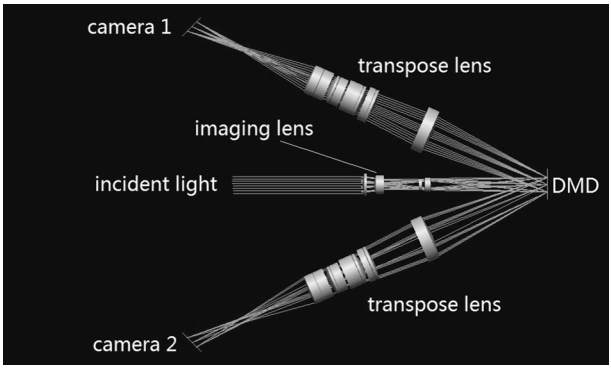

Fig. 1 Optical structure of the system

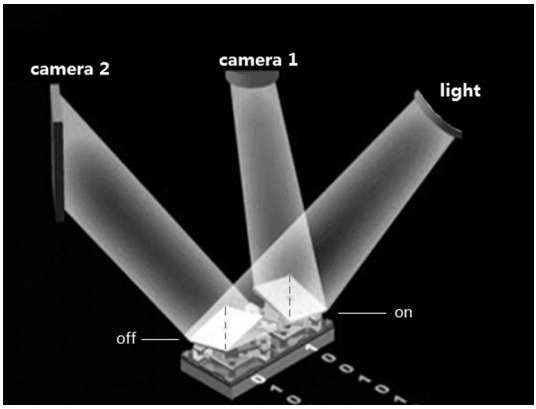

Fig. 2 DMD work mode

2 Binocular HDR imaging system using DMD

The system is mainly composed of an imaging lens, transpose lens, DMD, cameras, and a computer. The optical structure of the system is shown in Fig. 1. First, the high dynamic scene (or the incident light) passes through the imaging lens onto the DMD; it is then modulated into two new scenes by the DMD. Each scene is projected on its corresponding camera through the transpose lens. Afterwards, the cameras transport the captured images to the computer, which reproduces them so that they can be observed by the naked eye. If the reproduced scenes do not meet our requirements, the computer controls the DMD and the camera to adjust the scene once again, and two new images are captured. This process loops until the reproduced scenes meet our requirements. It is noteworthy that the projection relationship of the DMD plane and the incident light, and of the reflected light and the camera sensor, are all inclined, which causes a special distortion in the system. Solving this will be discussed in Sect. 3.

A DMD is made up of millions of individually controlled micro-mirrors. Each micro-mirror can be turned on or off by controlling the voltage of its corresponding address. Each DMD is responsive to a pixel point of the cameras. Figure 2 shows the work mode of the DMD in the system. A beam of parallel light projects on the DMD and is reflected in two ways. In each way, there exists a camera to capture the scene. When the micro-mirror is

turned on, the incident light is reflected to camera 1, and its corresponding pixel in camera 1 captures the scene, but the corresponding pixel in camera 2 does not. Likewise, when the mirror is turned off, the incident light is reflected to camera 2, and its corresponding pixel in camera 2 captures the scene, but that in camera 1 does not. During one frame, the micro-mirrors flip several times. Therefore, the time ratio of a mirror in an on state is its corresponding pixel-point-adjusting weight in camera 1; the time ratio of a mirror in an off state is its corresponding pixel-point-adjusting weight in camera 2. During one frame, the product of the time ratio of a mirror in an on state and the display width of the DMD is its gray value in the mask image. Each point of the mask image can be set at any gray value, so the mask image can be set whatever value is desired.

In a normal HDR system based on a DMD, the dynamic range of the system DR_{sys} consists of the dynamic range of the camera (DR_{Camera}) and the dynamic range of the DMD (DR_{DMD}), which can be expressed as

$$DR_{sys} = DR_{Camera} + DR_{DMD}. \tag{1}$$

In the proposed binocular HDR system, the two cameras can be set at two different integral times, so that the dynamic range of the system can be extended. Assuming that DR_{Ratio} is the dynamic range of the ratio of the two cameras' integral time, (1) can be rewritten as

$$DR_{sys} = DR_{Camera} + DR_{DMD} + DR_{Ratio}. \tag{2}$$

The DMD used is manufactured by Texas Instruments, Inc. (Product Code 0.7 XGA) and has a frame rate 10 frames/s in the case of 11 bits. The camera is a CMOS camera (Product code CIS-2521) with a dynamic range of approximately 83 dB.

For the same intensity incident light, N different kinds of light intensity can be generated by adjusting the light with different N weights of DMD. When incident on CMOS image sensor, N kinds of image gray level will be generated.

In theory, the response of CMOS image sensor is linear with N light-adjusting weights. When the maximum weight of DMD is 1, all light passes through. When the adjusting weights of DMD is minimum, such as 1/2048, it means 1/2048 light intensity passes through. So, DR_{DMD} is determined by the maximum and minimum adjusting weights of the DMD (r_{max} and r_{min}). In our system, the DMD has been extended to 11 bits (Wang et al. 2014); thus, $r_{max} = 1$ and $r_{min} = 1/2048$. DR_{DMD} can be expressed as

$$DR_{DMD} = 20log\left(\frac{r_{max}}{r_{min}}\right) = 66dB. \tag{3}$$

DR_{Ratio} is determined by the ratio of the integration time of the two cameras. In the HDR system the ratio of the integration time of the two cameras can reach at least 1000 under the premise of considering the performance of the camera and the image quality. Then, DR_{Ratio} can be expressed as

$$DR_{Ratio} = 20log(1000) = 60dB\,, \tag{4}$$

and thus the theoretical dynamic range of the system is 209 dB according to (1).

3 Pixel-matching algorithm

In the proposed system, the resolution of the DMD is 1024×768, which is less than that of the camera (1280×1024). Therefore, the final image captured by the camera has a 1024×768 DMD image in its center; and the rest of the pixels around the DMD image

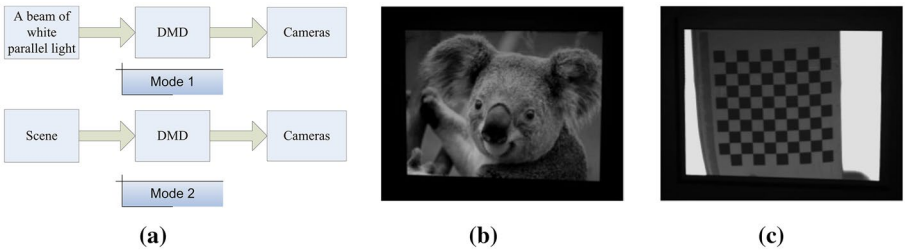

Fig. 3 Imaging results

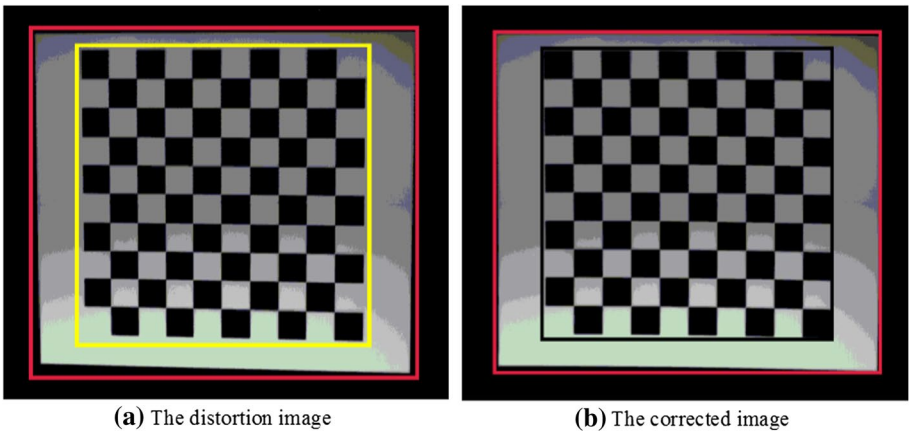

Fig. 4 Distortion-correction effect using Zheng-you's method

are all black. By using the phase property of the moire fringe, the size error between the micromirror and camera pixel can be adjusted to less than 0.04 pixel (Ri et al. 2006).

As shown in Fig. 3, our system has two work modes. In Mode 1, a collimated beam of light goes through the imaging lenses to the DMD, the DMD reflects the light to the two transpose lenses, and finally the two cameras capture two images. Because the parallel light is white, the central parts of the two camera images solely depend on the flip time of the micromirrors in the DMD, as if the DMD draws an image on a white board. Figure 3b shows an instance in which the DMD draws a koala with Mode 1. This mode is designed for distortion calibration. In Mode 2, it is a natural scene that goes through the imaging lenses. This means that the final camera images depend on the scene and the flip time of the micromirrors in the DMD. The DMD plays the role of a light modulator. In this mode, the final goal is to obtain the details of all the targets in the scene, regardless of the targets' brightness. Figure 3c is a checkerboard captured by the system in Mode 2.

We can also see that there is some distortion in the picture that will influence the accuracy of the light adjustment. In order to achieve pixel-level adjustment control, the micromirrors on the DMD should correspond with the pixels of the two cameras.

Figure 4 shows the distortion-correction result using Zheng-you's method (Zhang 1999). In the picture some color boxes are used as reference lines to contrast with the correction effect. It can be seen that the image after correction has been improved to some extent, but there are

still some distinct distortions in the bottom left-hand corner. Thus, the corrected image cannot meet the pixel-level requirements of the system.

Therefore, we propose a novel method for distortion correction, which quickly and accurately completes the calibration and matching procedure. The proposed method uses DMD to display the calibration template; hence, the system completes the calibration itself without additional templating. Figure 5 shows the template pattern displayed by the DMD. It is composed of three differently sized rectangular frames and a cross-hair. The pattern is symmetrical to the center of the image. The linewidth measures 1 pixel and the coordinates of every corner point is known. The gray value of the template can be customized on the premise that there is a clear contrast between the lines and the background. Using the template's gray value, the contrast before and after correction can be directly observed. In order to express the distortion-correction results more intuitively in the rest of this section, the corners of the template are numbered.

Much research has been conduction in the field of distortion correction. Distortion models can be expressed by a polynomial and the tilt distortion can be expressed as Li (2011)

$$\begin{cases} \delta_{xl} = a_0 x + a_1 y + a_2 xy + a_3, \\ \delta_{yl} = b_0 x + b_1 y + b_2 xy + b_3. \end{cases} \tag{5}$$

Among these, δ is the ideal coordinate and (x,y) are the coordinates of the distortion image. In the process of solving the distortion model of the system, we only discuss the tilt distortion at first. After correcting the tilt distortion of each rectangle, we extract the coordinate values of the 25 corners in the calibration template and then establish a mapping function Δ with the ideal corner coordinates. Experiments show that the mapping function is related to the region where the coordinates are located, and can be approximately expressed as a quadratic curve without considering the higher order terms. In this work, the Δ can be expressed as (6):

$$\begin{cases} \Delta_x = c_0 x^2 + c_1 x + c_2, \\ \Delta_y = d_0 y^2 + d_1 y + y_2, . \end{cases} \tag{6}$$

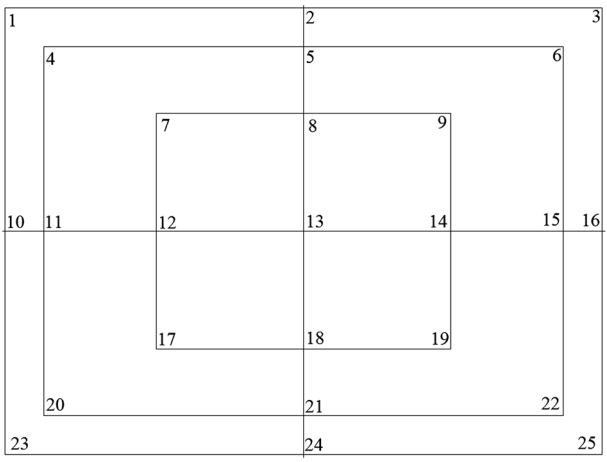

Fig. 5 Calibration template

Then, combining (5) and (6), the final distortion model can be expressed as (7) ignoring higher-order terms:

$$\begin{cases} \delta_x = \delta_{xl} + \Delta_x = A_0x^2 + A_1x + A_2y + A_3xy + A_4, \\ \delta_y = \delta_{yl} + \Delta_y = B_0y^2 + B_1x + B_2y + B_3xy + B_4. \end{cases} \tag{7}$$

Assuming that the distortion images collected by the cameras are $f_1(x_1, y_1)$ and $f_2(x_2, y_2)$, the ideal image that does not exhibit distortion is $g(u, v)$, and the coordinates of the same control point in the images before and after correction are (x_1, y_1), (x_2, y_2), and (u_1, v_1) ,(u_2, v_2). Letting $h(x, y)$ represent the distortion model (7), the relationship between (x, y) and (u, v) can be expressed as

$$\begin{cases} u_1 = h_1(x_1, y_1), \\ v_1 = h_2(x_1, y_1), \\ u_2 = h_3(x_2, y_2), \\ v_2 = h_4(x_2, y_2). \end{cases} \tag{8}$$

The process of correcting the distortion image is to traverse each point in the distortion image to obtain its corresponding point and to assign it according to (7). However, in this method the relationships between the points in the two images are not one to one. There may be two or more points in the distorted image mapped to the same point after correction, which makes some points of the corrected image being to be assigned several times while some are not assigned. In the proposed method, we exchange the ideal image and the distortion image, which means that we regard the ideal image as the new distortion image and the distortion image as the new ideal image. The distortion image is produced by the ideal image after distortion. Neglecting higher-order terms, the final distortion mode can be expressed as

$$\begin{cases} x_1 = a_0u_1^2 + a_1u_1 + a_2v_1 + a_3u_1v_1 + a_4, \\ y_1 = b_0v_1^2 + b_1u_1 + b_2v_1 + b_3u_1v_1 + b_4, \\ x_2 = c_0u_2^2 + c_1u_2 + c_2v_2 + c_3u_2v_2 + c_4, \\ y_2 = d_0v_2^2 + d_1u_2 + d_2v_2 + d_3u_2v_2 + d_4. \end{cases} \tag{9}$$

A collimated beam of light is illuminated in the system and the calibration template is displayed by the DMD; then, the distortion images of the two cameras are obtained. According to the distortion model, we acquire the distortion parameters of the two cameras and complete the correction. The results are shown in Fig. 6, in which it can be seen that there are very serious distortions before correction. The top corners exhibit very distinct tilt distortion and the images exhibit eccentric distortion. After correction, the distortions have been nearly eliminated.

In order to accurately analyze the correction results, we obtain the corner coordinates of the four images. Assuming the coordinates before correction are (x, y) and the coordinates after correction are (x', y'), the deviation is expressed as

$$deviation = \sqrt{(x - x')^2 + (y - y')^2}. \tag{10}$$

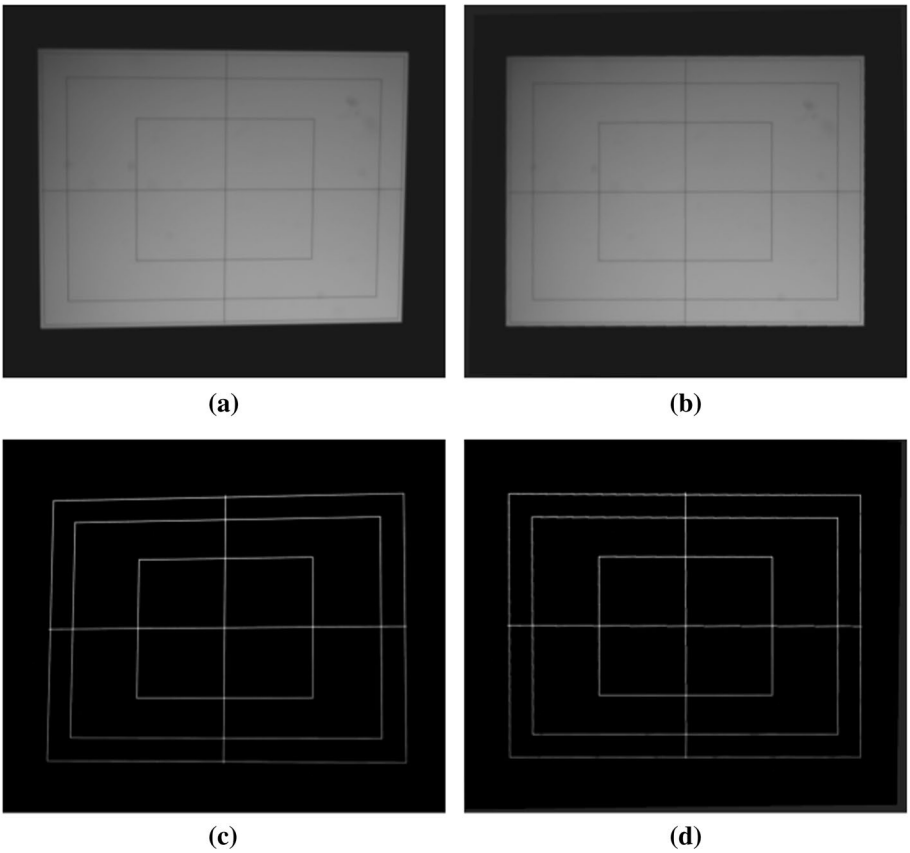

Fig. 6 Distortion-correction results. Image (**a**) is collected by camera 1 before calibration and image (**c**) is collected by camera 2 before calibration. Images (**b**) and (**d**) are the correction results of (**a**) and (**c**)

The errors of every corner before and after correction are shown in Tables 1 and 2, respectively.

It is clear that the average pixel deviation of the distortion image is approximately 8.5 pixels and the maximum deviation is 30.48 pixels. After correction, the average deviation decreases to less than 1 pixel and the maximum deviation is 1.41 pixels. In order to verify the matching accuracy of the two corrected images captured by the two cameras, the pixel deviation of the corner points between Fig. 7b, d is presented in Table 3.

As can be seen from the table, the average deviation of the two corrected sensors is 0.48 pixels and the maximum deviation is less than 1 pixel, which meets the accuracy requirements of the imaging system.

4 Light-adjusting algorithm

One of the strengths of using a DMD to extend the system's dynamic range is that it can be designed to achieve different adjusting algorithms on the same hardware platform. In order to describe the model, we make the following definitions:

Table 1 Error analysis of distortion correction of camera 1

No.	Deviation before correction (pixels)	Deviation after correction (pixels)	No.	Deviation before correction (pixels)	Deviation after correction (pixels)
1	5.83	0.01	14	5.66	0.81
2	11.18	0.80	15	7.70	0.17
3	30.48	0.04	16	8.94	0.89
4	4.47	1.38	17	5.10	1.40
5	11.40	1.34	18	6.71	0.83
6	23.43	1.22	19	8.25	0.71
7	1.00	1.23	20	1.00	0.02
8	2.24	0.82	21	7.07	0.97
9	10.77	1.23	22	9.06	0.88
10	5.83	0.96	23	2.83	0.16
11	5.10	1.33	24	5.66	0.91
12	5.10	0.26	25	10.20	0.10
13	7.07	0.20			
Average deviation before correction		8.06	Average deviation after correction		0.75

Table 2 Error analysis of distortion correction of camera 2

No.	Deviation before correction (pixels)	Deviation after correction (pixels)	No.	Deviation before correction (pixels)	Deviation after correction (pixels)
1	5.66	0.18	14	9.22	1.27
2	11.70	0.84	15	24.41	0.82
3	9.43	0.53	16	3.00	0.05
4	9.85	0.92	17	11.66	0.99
5	5.39	0.83	18	9.06	0.82
6	5.39	0.83	19	11.00	0.02
7	5.39	0.97	20	9.22	0.91
8	12.53	0.05	21	12.08	0.90
9	2.83	1.29	22	6.71	0.92
10	12.37	0.81	23	6.08	0.84
11	7.07	0.80	24	13.42	1.30
12	17.00	0.01	25	5.66	0.69
13	1.41	0.76			
Average deviation before correction		9.10	Average deviation after correction		0.73

$$I(x, y) = u(E(x, y))T\,, \tag{11}$$

$$r(x, y) = \frac{t(x, y)}{T}. \tag{12}$$

Table 3 Pixel deviation of the two corrected cameras

No.	Deviation	No.	Deviation	No.	Deviation	No.	Deviation
1	0.04	8	0.02	15	0.28	22	0.35
2	0.93	9	0.79	16	0.85	23	0.81
3	0.12	10	0.59	17	0.45	24	0.74
4	0.62	11	0.20	18	0.99	25	0.52
5	0.90	12	0.15	19	0.21		
6	0.15	13	0.61	20	0.14		
7	0.83	14	0.51	21	0.16		
Average deviation				0.48			

where $I(x, y)$ represents the real gray value of high dynamic scene with exposure time of T, $E(x, y)$ is the energy value of high dynamic scene imaging on DMD, $u()$ denotes a series of photoelectric conversion processes that convert the brightness value to the gray value of the image in unit time, $t(x, y)$ is the effective time of micromirror modulation of DMD at point (x, y), $r(x, y)$ represents the adjusting weight of its corresponding point (x, y), which is used to represent the attenuation of the scene.

In the proposed binocular HDR imaging system, $r_1(x, y)$ is the adjusting weight of camera 1 and is related to the time of its corresponding micromirror in the on state; $r_2(x, y)$ is the adjusting weight of camera 2 and is related to the time of its corresponding micromirror in the off state. The relationship between r_1 and r_2 can be expressed as $r_1 + r_2 = 1$. Taking the integral time of camera 1 (T_1) as a reference, the integral time of camera 2 can be expressed as T_2. Assuming that the images collected by the two cameras are $f_1(x, y)$ and $f_2(x, y)$, and ignoring the influence of the PSF (point spread function), the light-adjusting model can be expressed as

$$\begin{cases} f_1(x,y) = I(x,y) \cdot r_1(x,y) = I(x,y) \cdot R_1(x,y), \\ f_2(x,y) = I(x,y) \cdot r_2(x,y) \cdot \alpha = I(x,y) \cdot R_2(x,y), \\ \alpha = \dfrac{T_2}{T_1} \end{cases} \tag{13}$$

where α is the ratio of exposure time between camera 2 and camera 1.

Therefore, the original scene can be recovered by

$$I(x,y) = f(x,y)/R(x,y). \tag{14}$$

where f represents f_1 and f_2, and R represents R_1 and R_2.

The dynamic range of the recovered scene is too high, and hence it cannot be represented on the display. The tone-mapping operator (TMO) is therefore adopted to represent the scene (Reinhard et al. 2010). The more samples of the scene are acquired, the more accurately can the scene data be recovered. However, increased sampling will increase computation time, so a quick and accurate algorithm is needed. To find a proper adjusting algorithm, four groups of sampling experiments were designed to recover a highly dynamic scene, according to the rules shown in Table 4. In this work, sampling times represent the times of multiple imaging based on the number of light-adjusting weights. Such as, the adjusting weights are 1, 1024/2048, 512/2048, 256/2048, 128/2048, 64/2048,

Table 4 Sampling rules

No.	Sampling times	Adjusting weight	Entropy
1	12	$1/2048, 2/2048, 4/2048, \ldots, 2048/2048$	10.7193
2	6	1/2048, 4/2048, 16/2048, 256/2048, 1024/2048, 2048/2048	10.5331
3	4	1/2048, 16/2048, 256/2048, 2048/2048	10.3605
4	2	1/2048, 2048/2048	8.3556

32/2048, 16/2048, 8/2048, 4/2048, 2/2048, 1/2048 (total 12), then the sampling times is 12. To quantitatively compare the recovery results of the above four experiments, image entropy was introduced (Liang and Hong 2008). It can be seen that with the decrease in the number of samplings, the information content is gradually reduced and the quality becomes worse.

In this paper, we introduce a novel light-adjusting algorithm for a highly dynamic scene in which the brightness of the targets remains relatively stable. The algorithm contains several steps, as follows:

1. Initialize the DMD and set $r_1 = 1/2048$, $r_2 = 2047/2048$. Set the minimum adjusting weight as 1/2048, the maximum adjusting weight as A and the entropy threshold is Th.
2. Adjust the integration time of camera 1 and camera 2, respectively. Adjust the integration time of camera 1 so that the camera can observe the details of the bright target and adjust the integration time of camera 2 to observe the details of the dark target. The ratio of the integration time of the two cameras is α. Set the integration time of camera 1 as a fixed value T_1 and let the integration time of camera 2 to be adjustable.
3. Preset all of the adjusting weights as 1/2048, 2/2048, 4/2048, 8/2048 (total N). Go through all the adjusting weights for r_1. By adjusting the micromirror and the integration time of camera 2, the adjusting weight can be set at any value.
4. Collect two images whose adjusting weight r_1 are 1/2048 and A, then recover the scene and calculate its entropy. If the entropy is above the threshold Th, then the adjusting work is done and we obtain the recovered scene according to (14); else go to step 5).
5. Double the sampling time and recover the scene. Calculate the entropy of the newly recovered scene. If the entropy is above Th, then the adjusting work is done and we obtain the recovered scene; else go to step 5).

In this system, we will select the threshold Th according to the performance of the camera and the quality of the image. Different scenes should select different thresholds. In this work, we use different weights of global DMD to obtain multiple images of the current scene, and calculate the entropy of these images. We select the threshold Th based on these values by hand. Global DMD means the $r(x, y) = r$ for all the points (x, y).

5 Experiments

The binocular HDR imaging system shown in Fig. 7 is designed to better observe highly dynamic scenes. That is to say, through this system, several targets with great differences in brightness can be clearly observed simultaneously. Therefore, the dynamic

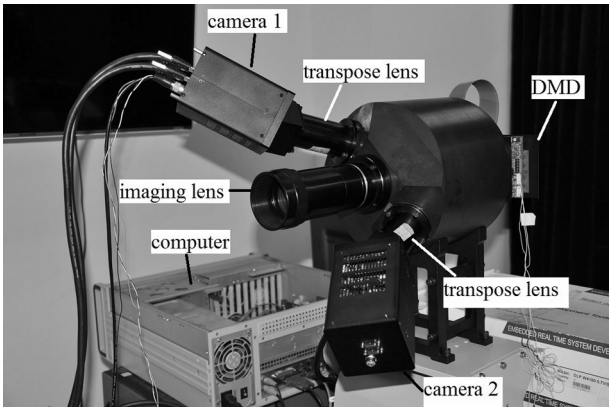

Fig. 7 Binocular HDR imaging system

range and imaging quality of the system are of the most concern. Meanwhile, it should be guaranteed that the adjustment accuracy of system is in a reasonable range. Applying the proposed method, several experiments were conducted to verify the adjustment accuracy, dynamic range, and imaging quality of the system.

5.1 Adjustment accuracy of the system

The DMD is the core device for realizing the adjustment process, and the adjusting weight is determined by its state time in a frame. The light-adjusting accuracy of the system includes two aspects: (1) the matching accuracy between the pixels of the sensors and the micromirrors in the DMD, and (2) the access between the adjusting weight of the DMD and the attenuation degree of the real scene. The first aspect was verified in Sect. 3. An experiment was designed to verify the accuracy of the second aspect.

In this experiment, we used a DMD to modulate a scene with high brightness and calculated the gray value of each adjusting weight. The results are presented in Table 5 and the response curve of the gray value and adjusting weight is shown in Fig. 8.

We can see from the table and figure that the gray value of the scene grows with increasing adjusting weight and the multiple of the increase is roughly the same, and the response curve between them is approximately linear. This experiment proves that the system satisfies the requirements of the light-adjusting accuracy in measuring a highly dynamic scene.

Table 5 Data from experiments on light-adjusting accuracy

Adjusting weight	Gray value	Adjusting weight	Gray value
1/2048	458	64/2048	32,833
2/2048	913	128/2048	65,905
4/2048	1853	256/2048	131,902
8/2048	3823	512/2048	264,046
16/2048	7933	1024/2048	529,217
32/2048	16,253	2048/2048	1,058254

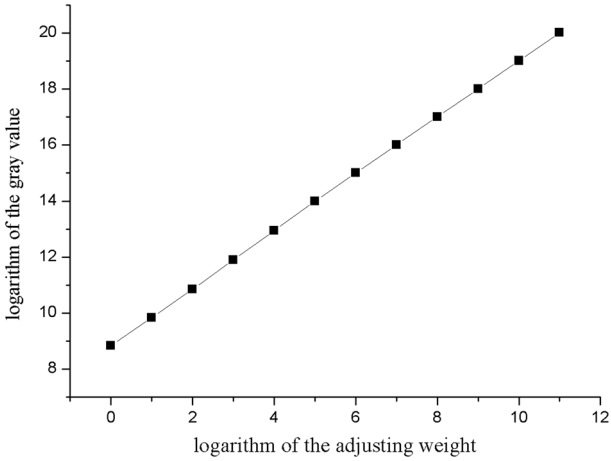

Fig. 8 Response curve of adjusting weight and gray value

5.2 Dynamic range of the system

To test the dynamic range of the system, a searchlight and a high-brightness LED lamp are used as the light source. The searchlight is shown in Fig. 9, and a black shade which has two same light holes is arranged in front of the searchlight. The two holes are of the central symmetry so that we can believe the light from the two holes is equal brightness. We place a attenuation slice in front of one hole and the attenuation rate is 2000 times. The illumination of the two holes is 994,700 lx and 500.2 lx, the difference between them is 1988.6 times and that is similar to the attenuation rate. We use the two holes as the bright target and normal target of the scene. Figure 10 shows the LED lamp, its illumination is 968700 lx which similar to the searchlight. We arrange a set of attenuation slices in front of the LED lamp and use it as the dark target, owing to the limitations of the experimental conditions,

(a) hole 1 **(b)** hole 2

Fig. 9 The searchlight in the high dynamic scene

Fig. 10 The LED lamp in the high dynamic scene

the attenuation rates of the slices are adjustable 500, fixed 1000, and fixed 2000; thus, the maximum attenuation rate is $500 \times 1000 \times 2000 = 1$ billion, Therefore the dynamic range of the whole high dynamic scene can be computed as $20\,\lg(10^9)$ dB $= 180$ dB.

In this experiment, the maximum attenuation rate is set to 1 billion, and then we use the system to image the scene. The finally recovered high dynamic scene is shown in Fig. 11. We can see the details of the three targets and the background of the scene from Fig. 11 so that we can safely draw the conclusion that the dynamic range of the system is more than 180 dB.

5.3 Imaging quality of the system

The ultimate goal of this system is to obtain information on both the bright and dark targets in highly dynamic scenes simultaneously. Two experiments were conducted to test

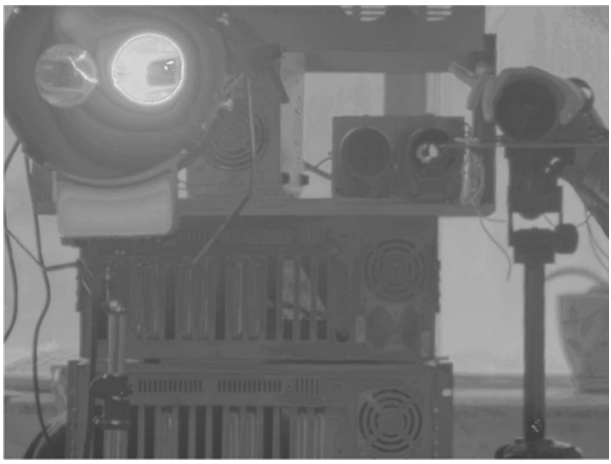

Fig. 11 Collected images of dynamic range verification experiment

the image quality after adjustment, i.e., to show whether the details of the bright and dark targets can be easily observed by the naked eye.

5.3.1 Light-adjusting experiment on single bright target

A single bulb consisting of three LED lamps was chosen as the single bright target; a book with complex words and patterns was used as the dark target. The different sizes and gray values of the words and patterns in the book increase the difficulty of the adjustment work. However, whether they could be clearly distinguished after adjustment strongly reflects the performance of the proposed method. Figure 12 shows the images of the highly dynamic scene before and after adjustment. It is clear that before adjustment, because of the impact of the bright target, the gray values of the left-hand side of the book are extremely high, and most of the details are lost. After adjustment, however, both the details of the book and the three lamps can be clearly observed simultaneously. This experiment proved that the system effectively eliminates the influence of a single bright target on other dark targets in highly dynamic scenes, and that the details of both targets are well preserved.

5.3.2 Light-adjusting experiment on multiple bright targets

In this experiment, a lamp consisting of eight closely spaced LEDs was chosen as the highly dynamic scene. The eight LEDs are considered multiple bright targets and the lampshade is considered the dark target. The images of the highly dynamic scene before and after adjustment are shown in Fig. 13. Before adjustment, we cannot tell what the lamp is made of, but after adjusting the eight independent LEDs the lampshade, and even its texture, can all be observed clearly. This shows that the system accurately distinguishes multiple bright and dark targets, even though they are fairly close to each other.

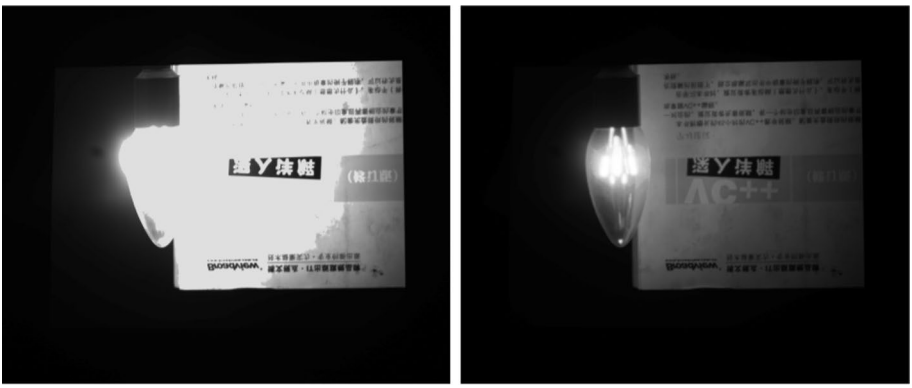

(a) the original scene **(b)** the recovered scene

Fig. 12 Images of highly dynamic scene before and after adjustment

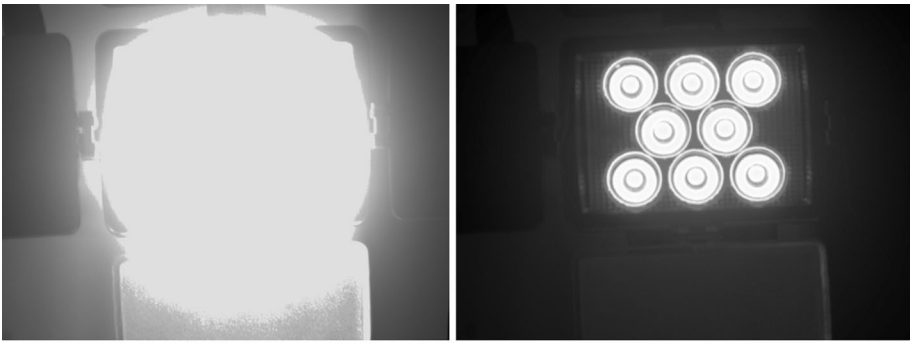

(a) the original scene **(b)** the recovered scene

Fig. 13 Images of highly dynamic scene before and after adjustment

6 Conclusions

According to the optical structure of a DMD, we introduced a novel binocular, highly dynamic light-adjusting system based on a DMD whose dynamic range can theoretically reach 209 dB. In order to realize the pixel matching of the two cameras, a simple but effective calibration template was designed for the special binocular system, and a fast, high-precision correction algorithm introduced. The matching algorithm achieves good correspondence between the pixels of the two cameras and the DMD micromirror, and the matching accuracy is better than 0.48 pixels. A binocular light-adjusting algorithm has also been put forward, which improves the speed of the system and achieves good imaging quality. In general, the adjusting speed is better than 1.67 fps. Experimental results show that the dynamic range of the system is above 180 dB, the adjustment accuracy of the system in terms of gray value can meet the requirements of highly dynamic measurements, and the quality of the recovered scene image is satisfactory, especially in some complex, highly dynamic scenes.

Acknowledgements This work was supported by the National High Technology Research and Development Program of China (Grant No. 2015AA7031010B).

Compliance with ethical standards

Conflict of interest We declare that we have no conflict of interest.

References

Guicquero, W., Dupret, A., Vandergheynst, P.: Multi-capture high dynamic range compressive imaging. In: 2013 Asilomar Conference on Signals, Systems and Computers, IEEE, pp. 143–147 (2013)

Härter, D., Müller, C., Reinecke, H.: Active triangulation metrology system with high dynamic range. J. Micro/Nanolithography MEMS MOEMS **10**(3), 13–18 (2011)

Huang, P.H., Maio, Y.H., Guo, J.I.: High dynamic range imaging technology for micro camera array. In: Signal and Information Processing Association Annual Summit and Conference (APSIPA), 2014 Asia-Pacific, IEEE 1–4 (2014)

Kavadias, S., Dierickx, B., Scheffer, D., Alaerts, A., Uwaerts, D., Bogaerts, J.: A logarithmic response cmos image sensor with on-chip calibration. IEEE J. Solid-State Circuits **35**(8), 1146–1152 (2000)
Lai, L.W., Lai, C.H., King, Y.C.: A novel logarithmic response cmos image sensor with high output voltage swing and in-pixel fixed-pattern noise reduction. IEEE Sens. J. **4**(1), 122–126 (2004)
Li, Y.: Local correction approach for inclined and distortional VLP image. Jisuanji Gongcheng yu Yingyong (Computer Engineering and Applications) **47**(17), 10–12 (2011)
Liang, J., Hong, Zl: Auto-exposure algorithm for scenes with large dynamic range. Opto-Electron. Eng. **5**, 89–92 (2008)
Mann, S., Picard, R.: On Being 'Undigital' with Digital Cameras: Extending Dynamic Range by Combining Differently Exposed Pictures, p. 7 (1996)
Mannami, H., Sagawa, R., Mukaigawa, Y., Echigo, T., Yagi, Y.: Adaptive dynamic range camera with reflective liquid crystal. J. Vis. Commun. Image Represent. **18**(5), 359–365 (2007)
Nayar, S.K., Branzoi, V.: Adaptive dynamic range imaging: optical control of pixel exposures over space and time. In: Computer Vision, 2003. Proceedings. Ninth IEEE International Conference on, IEEE, pp. 1168–1175 (2003)
Reinhard, E., Heidrich, W., Debevec, P., Pattanaik, S., Ward, G., Myszkowski, K.: High Dynamic Range Imaging: Acquisition, Display, and Image-Based Lighting. Morgan Kaufmann, Los Altos (2010)
Reza, S.A., Riza, N.A.: High dynamic range variable fiber-optical attenuator using digital micromirrors and opto-fluidics. IEEE Photonics Technol. Lett. **21**(13), 845–847 (2009)
Ri, S., Fujigaki, M., Matui, T., Morimoto, Y.: Accurate pixel-to-pixel correspondence adjustment in a digital micromirror device camera by using the phase-shifting moiré method. Appl. Opt. **45**(27), 6940–6946 (2006)
Spivak, A., Belenky, A., Fish, A., Yadid-Pecht, O.: Wide-dynamic-range CMOS image sensors: comparative performance analysis. IEEE Trans. Electron Dev. **56**(11), 2446–2461 (2009)
Wang, Y.J., Chen, H.Z., Liu, Y.Y., Sun, H.H., Yang, Z.Y., He, S.W., et al.: Application of DMD to high dynamic scene image detection system. Opt. Precision Eng. **22**(9), 2508–2517 (2014)
Zhang, Z.: Flexible camera calibration by viewing a plane from unknown orientations. In: The Proceedings of the Seventh IEEE International Conference on Computer Vision, vol. 1. pp. 666–673 (1999)
Zhou, W., Shen, W.: Enhancement of dynamic range of FPA detector by using digital micro-mirror device. In: International Conference of Optical Instrument and Technology, International Society for Optics and Photonics, vol. 7156, p. 71562X (2008)